MATERIALS
CHEMISTRY
FRONTIERS

View Article Online
View Journal | View Issue

Seeking value from biomass materials: preparation of coffee bean shell-derived fluorescent carbon dots *via* molecular aggregation for antioxidation and bioimaging applications†

Xinyue Zhang,‡ Hui Wang,‡ Chunhui Ma, Na Niu, [ID] Zhijun Chen,* Shouxin Liu [ID] Jian Li and Shujun Li [ID]*

Bifunctional carbon dots have shown a large amount of potential in bioimaging and antioxidation applications. However, the hydrothermal method for the preparation of bifunctional carbon dots requires a high energy input and an expensive setup. Moreover, this method breaks down sensitive compounds in the raw materials and could decrease the antioxidation ability of the resulting carbon dots. Here, phenolic extracts of coffee bean shells were used to prepare carbon dots *via* a cheap, energy-saving, mild molecular aggregation method. The as-prepared carbon dots were characterized by TEM, HPLC, XPS and Raman spectroscopy. The carbon dots had a diameter ranging from 1 to 5 nm and mainly contained three kinds of phenolic compounds including 3,4,5-trihydroxybenzoic acid, 3,4-dihydroxybenzaldehyde and 3,4-dihydroxybenzoic acid. The carbon dots demonstrated a strong antioxidation capacity, which was comparable to the commercially available butylated hydroxytoluene. The EC_{50} of the carbon dots was 110 μg mL^{-1}. The carbon dots had a pH-/excitation-dependent fluorescence. The as-prepared carbon dots also showed anti-bleaching fluorescence, which was better than that of the commercially available 4′,6-diamidino-2-phenylindole. Based on this finding, the excellent biocompatibility of carbon dots enabled them to be successfully used for banana storage and imaging both cancer cell nuclei and tumors *in vivo*.

Introduction

Nanomaterials have shown great potential in antioxidation[1–5] and bioimaging applications.[6–18] Compared to other nanomaterials, carbon dots can be used for antioxidation and bioimaging applications due to several properties that they have demonstrated, such as good biocompatibility, cheap raw materials and easy preparation.[19–29] A few of these carbon dots have even shown both good antioxidation and bioimaging performance, which has great potential.[19,20] However, there are still some shortcomings in this area. For instance, most of the bifunctional carbon dots that were used for antioxidation and bioimaging were prepared through a hydrothermal method.[19,20] This preparation method required high temperature, which could destroy sensitive compounds in the raw materials that are of great importance for antioxidation.[30]

Key Laboratory of Bio-based Material Science and Technology of Ministry of Education, Materials Science and Engineering College, Northeast Forestry University, Hexing Road 26, Harbin 150040, P. R. China.
E-mail: chenzhijun@nefu.edu.cn, lishujun_1999@126.com

‡ These authors contributed equally to the paper.

In our previous report, a new method, molecular aggregation, was developed to prepare lignin-based carbon dots.[31] This method did not require toxic reagents, heating or an expensive setup and avoided breaking down the chemical structure of the raw materials.[30,31] These points reminded us that biomass materials that contain phenolic compounds might be very suitable for the preparation of bifunctional carbon dots with good performance for antioxidation and bioimaging *via* molecular aggregation, as this preparation method would retain the phenolic compounds with strong antioxidation capability in the carbon dots.[32,33] Coffee bean shells, as a byproduct of the coffee industry, are often discarded, despite containing many phenolic compounds.[34,35] If these phenolic compounds can form carbon dots *via* molecular aggregation (CS-CDs), these as-prepared CS-CDs should be ideal materials for antioxidation and bioimaging. Specifically, CS-CDs can be prepared without toxic reagents, which can ensure their good biocompatibility. In addition, the as-prepared CS-CDs could have a high antioxidation capacity, as phenolic compounds could be retained during the preparation. Also, converting the under evaluated biomass materials to functional nanomaterials can provide an opportunity for their high value-added application.[36–40] These advantages
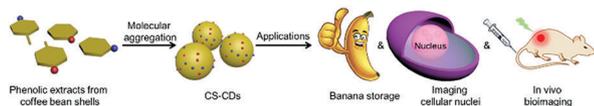
Fig. 1 Schematic illustration of the preparation of CS-CDs from coffee shell beans and applications of CS-CDs in banana storage, imaging of cellular nuclei and *in vivo* bioimaging.

might allow CS-CDs to be antioxidants for fruit storage and bioimaging probes. Although there could be potential advantages and applications by converting phenolic extracts, such as 3,4,5-trihydroxybenzoic acid, 3,4-dihydroxybenzaldehyde and 3,4-dihydroxybenzoic acid from coffee bean shells to CS-CDs *via* molecular aggregation, no attention has been given to this area. Inspired by these points, we explored a method of preparing CS-CDs *via* molecular aggregation from the phenolic extracts of coffee bean shells (Fig. 1). Then, CS-CDs were used for banana storage based on their antioxidation ability, and imaging of cellular nuclei and *in vivo* bioimaging (Fig. 1).

Experimental section

Chemicals and materials

Coffee bean shells were provided by the Kanghe Company, Yunnan, China. Sodium hydroxide, sulfuric acid, methanol and 4′,6-diamidino-2-phenylindole (DAPI), and 1,1-diphenyl-2-picrylhydrazyl (DPPH) were purchased from Kermel (Tianjin, China) and Solarbio (Beijing, China); polyvinyl alcohol (PVA, average degree of polymerization, 1750 ± 50) was obtained from Sigma-Aldrich (Shanghai, China), all the other solvents or reagents used in this paper were purchased from Kermel (Tianjin, China).

Instrumentation

Transmission electron microscopy (TEM) and high-resolution TEM images of CS-CDs were obtained using a JEM-2100 transmission electron microscope (JEOL, Ltd) at an accelerating voltage of 200 kV. Samples were ultrasonicated for 1 h before testing in an ice bath. The solution of CS-CDs was dropped onto a copper grid coated with an ultrathin carbon film and dried. The Raman spectra were recorded using a JY HR800 laser Raman spectrometer (Jobin Y von Horiba, France), with a 458 nm laser beam. Fourier transform infrared (FTIR) spectra were recorded using a Nicolette 6700 FT-IR spectrometer (Thermo Fisher Scientific, America) from 400 cm^{-1} to 4000 cm^{-1}, using the attenuated total reflection (ATR) method. X-ray photoelectron spectroscopy (XPS) was performed using a PHI 5700 spectrometer (Physical Electronics, America). UV-Vis absorption spectra were recorded using a TU-1900 UV-vis spectrometer (Persee, China). Fluorescence spectra were recorded using an LS-55 fluorescence spectrophotometer (PerkinElmer, Inc., Waltham, MA, USA), equipped with a 120 W xenon lamp as the excitation source. Fluorescence images were recorded using an Axio Imager A1 upright fluorescence microscope (Carl Zeiss AG, Oberkochen, Germany). Excitation wavelengths were in the range of 365,

450–490, and 546 nm. The cellular uptake by HeLa cells was observed using an SP8 confocal laser scanning microscope (Leica microsystems, Germany). HPLC was detected using an Agilent 1260 with an SDB-C18 column (250 mm × 4.6 mm, 5 μm).

Preparation of CS-CDs

Coffee bean shells (100 g) were stirred with 4% aqueous sodium hydroxide solution (500 mL) for 1.5 h. The undissolved solid residue was separated from the solution by vacuum filtration. The filtrate was collected and acidified to the point of precipitation (pH ∼ 2) using hydrochloride acid (0.5 M) solution. After allowing to stand overnight, the precipitate was collected by vacuum filtration, washed thoroughly with distilled water three times and then vacuum dried at 0.1 MPa and 50 °C. The dried precipitate was then dissolved in methanol/water (1 : 1/v : v) and dialyzed using a dialysis tube (M_w = 8000–14 000 mol g^{-1}). The sample outside the dialysis bag was denoted as coffee bean shell carbon dots (CS-CDs).

Measurement of total phenolics in CS-CDs

The Folin–Ciocalteu (FC) method was used to determine total phenolics in CS-CDs. Specifically, absorption of Folin–Ciocalteu (FC) in the presence of phenol at different concentrations ranging from 9.58 μM to 47.9 μM was measured at 760 nm. A linear equation was fitted from this absorption coefficient (y = 0.0118x + 0.0254, R^2 = 0.999). Meanwhile, CS-CDs were dissolved in distilled water (100 mL). The as-prepared CS-CD aqueous solution (4 mL), FC (3 mL) and 30 mL of distilled water were then added to a 50 mL volumetric flask. After 8 min, 10 mL of 20% Na_2CO_3 was added to the solvent with continuous stirring for 2 h in the dark at room temperature. The absorption coefficient of the as-prepared samples was measured at 760 nm. The phenolics in CS-CDs were calculated by absorption coefficient of CS-CDs at 760 nm and the fitted linear equation.

Radical scavenging activity (RSA)

The scavenging activity of CS-CDs to DPPH free radicals was evaluated by monitoring the reduction of DPPH induced by CS-CDs in methanol solution. In the tests, CS-CDs were added to 3 mL of DPPH (0.04 mg mL^{-1}) ethanol solution. The resulting decrease in absorption at 515 nm was measured. The RSA for DPPH was estimated using the following equation: inhibition (%) = $(A_C - A_0)/A_C$ × 100%, where A_C and A_0 refer to the absorbance of the DPPH at 515 nm in the absence and presence of CS-CDs, respectively. The EC_{50} (the half maximal effective concentration) value was calculated to determine the 50% inhibition of the radicals.

Banana experiment

Banana coating was fabricated by brushing banana with a PVA solution or a mixed solution of CS-CDs/PVA (0.5% according to the total mass of PVA). The coated bananas were stored at room temperature (room temperature = 23 °C). Photographs of the control bananas, PVA-coated and CS-CDs/PVA-coated bananas were taken on different days. The oxidation degree of bananas was determined by the area of black and number of black spots on the bananas.

Cell viability measurement

The effects of the newly prepared CS-CDs on cell viability were examined *in vitro* using 3-(4,5-dimethylthiazol-2-yl)-2,5-diphenyl-tetrazolium bromide (MTT) assays in L929 fibroblasts. The L929 fibroblasts were seeded onto a 96-well plate, with 6000–7000 cells in 200 μL of culture medium per well. The plate was then incubated at 37 °C for 24 h in the presence of 5% CO_2 to allow the cells to attach to the wells, and the cells were exposed to CS-CDs at different concentrations (0, 12, 25, 50, 100, 200 and 400 μg mL^{-1}) and incubated for another 24 h at 37 °C in the presence of 5% CO_2. MTT solution (20 μL, 5 mg mL^{-1}) was then added to each well, and after incubation at 37 °C for 4 h, the absorbance of each well was measured using a microplate reader, with 490 nm as the detection wavelength. The average readings and standard deviations were based on four samples, and all tests were performed in triplicate. Cell viability was calculated using the following equation: cell viability (%) = $A_{test}/A_{control}$, where A_{test} is the average cell viability in the presence of CS-CDs and $A_{control}$ is the average cell viability in the absence of CS-CDs (control experiment).

Cell culture and treatment

HeLa cells were seeded onto clean coverslips in 6-well culture plates. The cells were grown for one night as a monolayer and then incubated with the as-prepared CS-CDs (100 μg mL^{-1} in PBS, pH = 7.4) at 37 °C for 0.5 h, 1 h or 3 h. The cells were rinsed three times with phosphate buffered saline (PBS, pH = 7.4) and then fixed with 2.5% formaldehyde (1 mL well^{-1}) at 37 °C for 10 min. Nuclear labeling was carried out by staining the nuclei with DAPI solution (20 μg mL^{-1} in PBS, 1 mL well^{-1}) for 10 min. The cells were rinsed three times with PBS. The coverslips were placed on a glass microscope slide, and the samples were observed using a confocal laser scanning microscope.

In vivo imaging

All animal experiments were conducted in accordance with regulations of the He Nan Medical Research center. The tumor in the nude mouse was induced using HeLa cells. CS-CDs were dispersed in ultrapure water for injection. *In vivo* fluorescence imaging was performed using a NightOwl LB 983 three-dimensional small-animal imaging system. Nude mice were injected with CS-CDs (3 nmol) *via* the tail vein, and images were recorded before the injection and 10 min–24 h after the injection. The mice were euthanized, major tissue and organs were dissected 24 h post-injection and fluorescence images were obtained. Another nude mouse without dissection treated with CS-CDs under the same conditions was used to investigate the toxicity of CS-CDs to the mice.

Results and discussion

Physiochemical characterization

As a starting point of our research, CS-CDs were prepared *via* molecular aggregation. Initially, the phenolic compounds in the form of phenolic sodium were extracted from coffee shells
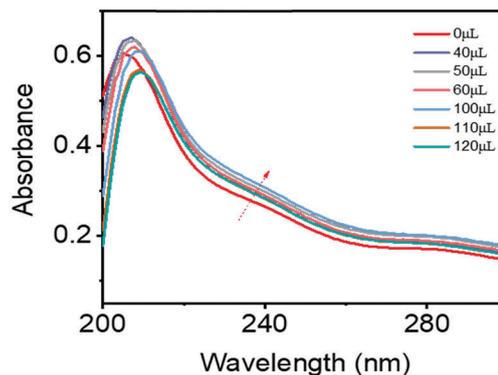

Fig. 2 UV-Vis absorption spectra of phenolic extract sodium salts upon the addition of HCl (0.1 M).

in an alkali. The phenolic sodium salts were well dispersed in the aqueous solution. Then, hydrochloric acid was added to systematically adjust the pH to 2. A red-shifted and increased absorbance was observed in the UV-vis spectra of the phenolic sodium salts upon the addition of acid, suggesting that J-type aggregates had formed.[41,42] These J-aggregates triggered molecular aggregation, which induced the formation of CS-CDs (Fig. 2). Subsequently, the chemical components of CS-CDs were analyzed by HPLC. From these extracted phenolic compounds, the HPLC analysis showed that CS-CDs contained 3,4,5-trihydroxybenzoic acid, 3,4-dihydroxybenzaldehyde and 3,4-dihydroxybenzoic acid (Fig. S1, ESI†). X-ray photoelectron spectroscopy (XPS) analysis showed that there was about 77.85% C, 21.28% O and 0.87% N in the CS-CDs. Some N in the CS-CDs might be attributed to peptides and lipids in the CS-CDs (Table 1).

After analyzing the components, the morphology and structure of the CS-CDs were investigated using a variety of analytical techniques. Transmission electron microscopy (TEM) images of CS-CDs (Fig. 3a) showed uniform dispersion and particle diameters of 1–5 nm (Fig. S2, ESI†). High-resolution TEM showed that most of the particles contained a well-resolved lattice spacing of 0.24 nm (Fig. 3b). The CS-CDs were also investigated in PBS buffer for the following bio-medical application. TEM images showed that CS-CDs had a diameter ranging from 1 to 5 nm with a well-resolved lattice spacing of 0.21 nm in PBS buffer, which was similar to their morphology in the aqueous solution. This result confirmed that the as-prepared CS-CDs had a good colloidal stability in PBS, which was necessary for their following application (Fig. S3, ESI†). The predominant carbon-lattice structure led to strong D and G bands in the Raman spectra of the CS-CDs (Fig. S4, ESI†), with an intensity ratio I_D/I_G of 0.56. In the Fourier transform infrared (FTIR) spectrum of the CS-CDs (Fig. 3c), the broad and intense peak at 3300 cm^{-1} and the peak at 1284 cm^{-1} were attributed to –OH bending and

Table 1 XPS data of CS-CDs

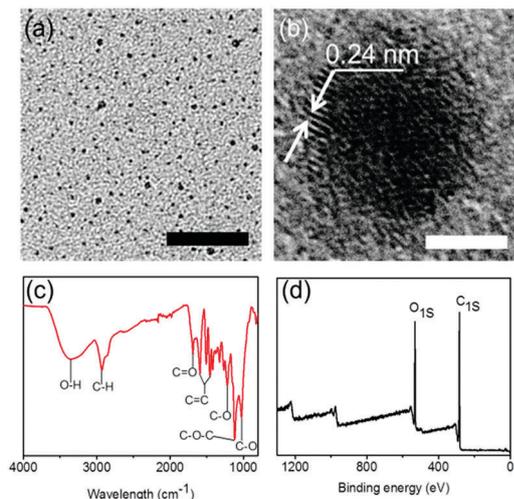| Name	Peak BE	FWHM (eV)	Area(P) CPS (eV)	Atomic (%)
C1s	284.64	1.45	61746.36	77.85
N1s	399.66	0.76	1147.49	0.87
O1s	532.42	1.91	41469.57	21.28

Fig. 3 (a) TEM image of CS-CDs, scale bar: 50 nm; (b) high resolution TEM image of CS-CDs, scale bar: 2 nm; (c) FTIR spectrum of CS-CDs; (d) broad XPS spectrum of CS-CDs.

C–O–C stretching vibrations, respectively. The bands at 1600 cm^{-1}, 1500 cm^{-1} and 1417 cm^{-1} were assigned to aromatic ring vibrations, and the peak at 1342 cm^{-1} was assigned to the stretching vibration of the C–O bond. The surface properties of the CS-CDs were also investigated using XPS (Fig. 3d). C1s analysis revealed three different types of carbon atoms: graphitic or aliphatic (C=C and C–C), oxygenated and hydrogenated (Fig. S5, ESI†). O1s analysis also revealed the presence of several types of oxygen atoms, including C–O–C, C=O/Ar–O–Ar and Ar–OH/O=C–O (Fig. S6, ESI†). All of the analytical results indicate that CS-CDs have a naturally conjugated structure, with passivated surfaces carrying aliphatic and aromatic hydroxyl groups. This type of structure satisfies the requirements for the luminescence emission of carbon dots.

Antioxidation ability

The CS-CDs consisted of phenolic compounds, and their surface was decorated with phenolic moieties, which enabled them to have antioxidation ability. The antioxidation ability of CS-CDs was determined by DPPH. After accepting a hydrogen radical, DPPH was converted into a stable DPPH-H complex, and the color of the solution changed from deep violet to light yellow (Fig. 4a). The radical-scavenging activity reached 85% when the concentration of CS-CDs was 0.16 mg mL^{-1}, and this activity was comparable to that of the commercially available butylated hydroxytoluene (Fig. 4b). By plotting the radical-scavenging activity against the concentration of CS-CDs, a linear relationship ($y = 428.24x$, $R^2 = 0.993$) was obtained for a CS-CD concentration ranging from 0 to 200 μg mL^{-1}. On this basis, the EC$_{50}$ was calculated to be 110 μg mL^{-1}. As a comparison, the EC$_{50}$ of the butylated hydroxytoluene was approximately 108 μg mL^{-1}. The CS-CDs showed strong antioxidation capability, which could be attributed to the high activity of phenolic compounds in the CS-CDs. In contrast to other preparation methods, which could destroy the structures of raw
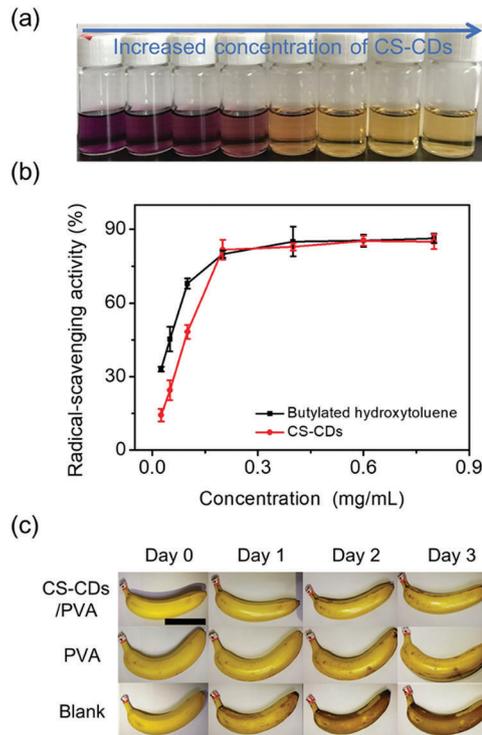

Fig. 4 (a) Images of DPPH in ethanol upon the addition of CS-CDs. (b) Scavenging of DPPH radicals as a function of CS-CD concentration and butylated hydroxytoluene. (c) Images of coated bananas on different days using CS-CDs/PVA (top), PVA (middle) and without coating (down). All images have the same scale; scale bar = 5 cm.

materials during the preparation of carbon dots, the phenolic extracts of coffee bean shells can be converted into CS-CDs *via* molecular aggregation without destroying their phenolic structures ($N_{\text{phenolic moieties}}/W_{\text{CS-CDs}} = 2.3$ mM g^{-1}, FC method), which enabled the CS-CDs to have high activity. $N_{\text{phenolic moieties}}/W_{\text{CS-CDs}}$ of the CS-CDs was still 2.3 mM g^{-1} after the ultrasonic treatment, indicating that the phenolics in the CS-CDs were quite stable. Due to their strong antioxidation capacity, CS-CDs were used as additives for banana storage. In this study, CS-CD-based coatings were compared to a control for banana storage. The surfaces of all bananas were initially yellow and unblemished (Fig. 4c). The bananas eventually decayed during storage, as evidenced by black spots (Fig. 4c). The appearance of bananas with the CS-CDs/PVA film coating showed less decay than that of the bananas both with PVA coating alone and without coating. These results confirmed that CS-CDs possess good oxidation capacity and can be used for fruit storage.

Optical properties

The optical properties of the CS-CDs were also investigated. A weak and broad absorption peak at 320 nm was attributed to the n → π* transition of carbonyl (C=O) groups, and a peak at 280 nm was attributed to the π → π* transition of alkene (C=C) groups. Following excitation at 320 nm, a peak centered at 380 nm was observed in the emission spectrum (Fig. 5a). The normalized photoluminescence (PL) spectrum (Fig. 5b) showed
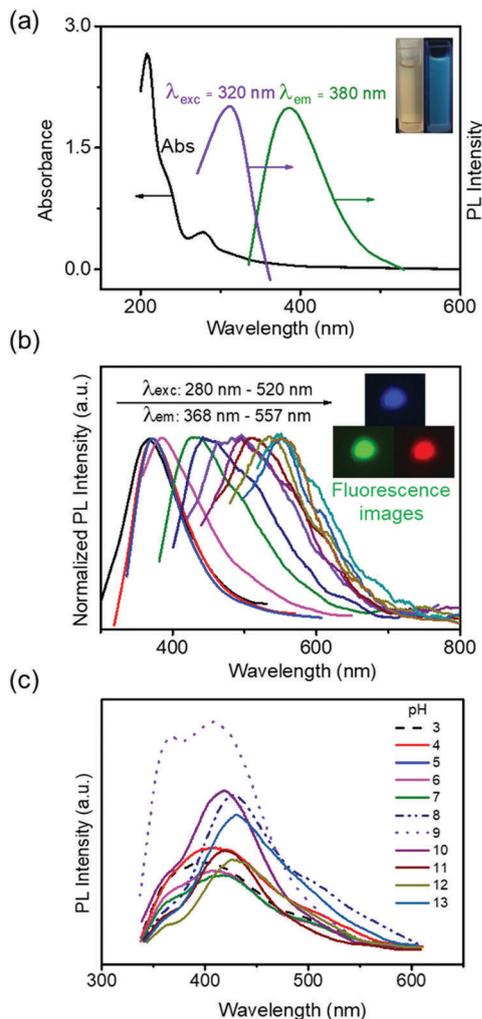
Fig. 5 Optical properties of CS-CDs. (a) Absorbance, excitation and emission spectra of the as-prepared CS-CDs dispersed in water. Inset: Photographs of CS-CDs in water under white light (left) and 365 nm UV light (right). (b) Normalized PL emission spectra showing the shift in emission wavelength from 368 to 557 nm as the excitation wavelength increased progressively from 280 to 520 nm. Inset: Fluorescence microscopy images of CS-CDs with UV, blue, and green light excitation. (c) Intensity of PL spectra of CS-CDs at pH values from 3 to 13.

an excitation wavelength-dependent shift in the wavelength of the emission peak (from 368 nm to 557 nm when the excitation wavelength was increased from 280 nm to 520 nm). Fluorescence images were also recorded to demonstrate the distinct emissions with different excitation wavelengths (Fig. 5b, inset). The HPLC results showed that CS-CDs contained mainly 3,4,5-trihydroxybenzoic acid, 3,4-dihydroxybenzaldehyde and 3,4-dihydroxybenzoic acid. These phenolic compounds that only contain a single aromatic ring cannot give rise to such a fluorescence emission. Thus, the fluorescence of CS-CDs might originate from the polydispersed J-aggregates inside.[43] The influence of pH on the emission of CS-CDs was also investigated (Fig. 5c). The maximum PL intensity occurred at pH 9 (Fig. 5c), and increasing the acid or base strength reduced the emission intensity (Fig. 5c), indicating that high concentrations of H+ or

OH− ions could interrupt and change the J-type aggregation of phenolic compounds in CS-CDs. The fluorescence stability was also investigated in aqueous solution and PBS buffer. The fluorescence emission of CS-CDs in PBS was lower than their fluorescence in aqueous solution (Fig. S7, ESI†). This result might be caused by the ions in PBS buffer that could quench the fluorescence of CS-CDs. Upon UV irradiation for 100 min, a decrease in fluorescence of only approximately 5% and 7% in the aqueous solution and PBS buffer, respectively, was observed for the CS-CDs (Fig. S8, ESI†). As a control experiment, exposing DAPI to UV light caused an obvious decrease in absorption (∼45%) (Fig. S8, ESI†). This result confirmed that CS-CDs had a good anti-photobleaching ability, indicating that they can be used as an alternative to DAPI for imaging cellular nuclei.

Bioimaging in vitro

MTT assays demonstrated that the as-prepared CS-CDs have excellent biocompatibility. HeLa cells remained viable when cultured for 24 h at 37 °C in the presence of increasing concentrations of CS-CDs. The cell viability was greater than 95%, even at a CS-CD concentration of 400 μg mL−1, indicating excellent biocompatibility (Fig. 6).

The excellent biocompatibility was the requirement for the following bioimaging experiment. HeLa cells were also used as a model cell line to investigate the cellular uptake and distribution of CS-CDs and to validate CS-CDs as agents for nuclear staining. Time-dependent fluorescence images of HeLa cells cultured with CS-CDs for 0.5 h, 1 h and 3 h are shown in Fig. 7 (top panel). Fluorescence images that were obtained using the commercially available nuclear staining reagent DAPI, which readily enters the cell nucleus, are shown in Fig. 7 (center panel). The merged images (Fig. 7, bottom panel) demonstrate that CS-CDs specifically target the nucleus of HeLa cells.

The fluorescence images obtained using CS-CDs are comparable with those obtained using DAPI. Importantly, CS-CDs are derived from a natural product and cost much less than DAPI and other commonly used nuclear dyes, indicating promise for commercial applications. CS-CDs show quite specific nuclear localization, which may be attributable, at least in part, to the small size of the CS-CDs. The diameter of the nuclear pore is approximately 8 nm, and CS-CDs, with a size distribution
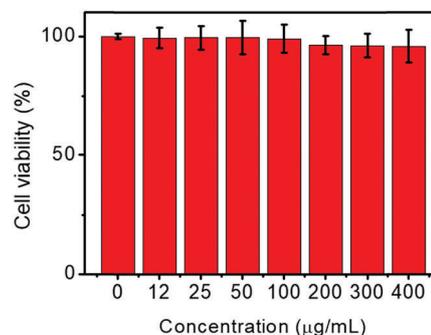

Fig. 6 In vitro L929 fibroblast cell viability after incubation with CS-CDs with different concentrations for 24 h.
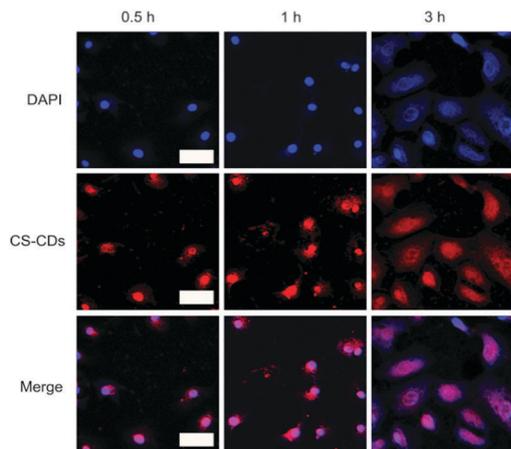
Fig. 7 Confocal laser scanning microscopy fluorescence images of HeLa cells after incubation with CS-CDs for different lengths of time. Top panel shows fluorescence images of nuclei stained with DAPI (405 nm excitation), center panel shows red fluorescence images of CS-CDs (514 nm excitation) and bottom panel shows merged images. Scale bar: 50 μm.

between 1 nm and 5 nm, can easily enter the nucleus. Phenolic groups on the surface of the CS-CDs may also contribute to nuclear localization. These phenolic groups may react specifically with DNA in the cell nucleus rather than with the cell membrane, the karyotheca or other organelles.[44]

Bioimaging *in vivo*

Encouraged by the result of cellular imaging, *in vivo* bioimaging was conducted. Without an injection of CS-CDs, fluorescent signals were not detected (Fig. 8a, 0 min). However, 10 min after the injection of CS-CDs, fluorescent signals were detected in the rear parts of the mice (Fig. 8a, 10 min). Subsequently, fluorescent signals were detected in the front parts of the mice (Fig. 8a, 30 min and 1 h). After 2 h, fluorescent signals were observed at the tumor positions of the mice (Fig. 8a, 2 h–24 h). To investigate the distribution of CS-CDs, dissection of mice was conducted after 24 h post-injection of CS-CDs. The images showed fluorescence in the liver and tumor, indicating the
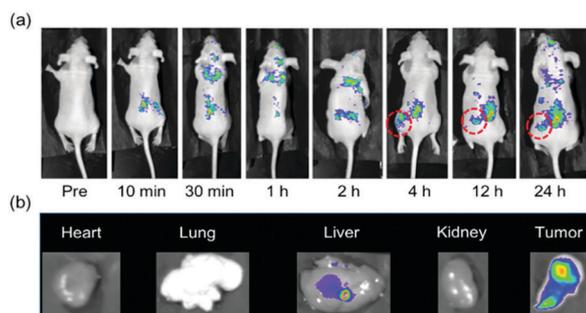

Fig. 8 (a) *In vivo* fluorescence imaging of nude mice after an intravenous injection of CS-CDs. CS-CDs were administered at a dose of 3 nmol per mouse *via* a lateral tail vein. Fluorescence images were acquired at 0 min, 10 min, 1 h, 2 h, 4 h, 12 h and 24 h. (b) Representative fluorescence images of dissected organs of a mouse after an intravenous injection of CS-CDs at a dose of 3 nmol per mouse. For all images, the excitation wavelength was 420 nm, and fluorescence emission was measured at 600 nm.

uptake of CS-CDs by these organs (Fig. 8b), but no fluorescence signals were collected in other organs (Fig. 8b). These results confirmed that CS-CDs aggregated in tumor positions and did not interrupt the kidney, lung or heart. Thus, fluorescent CS-CDs have great potential for *in vivo* bioimaging. Notably, the mice were still alive after injection for 6 days, which indicated that CS-CDs have good *in vivo* biocompatibility.

Conclusions

CS-CDs were prepared *via* a cheap, energy-efficient, mild molecular aggregation method that uses phenolic extracts of coffee bean shells. CS-CDs contained three kinds of compounds including 3,4,5-trihydroxybenzoic acid, 3,4-dihydroxybenzaldehyde and 3,4-dihydroxybenzoic acid. CS-CDs were well dispersed and had diameters in the range of 1–5 nm. The as-prepared CS-CDs showed a good antioxidation capacity that was comparable to that of the commercially used butylated hydroxytoluene (EC_{50} of CS-CDs = 110 μg mL^{-1}). The excellent antioxidation ability was employed for food storage. CS-CDs also showed pH-/excitation-dependent photoluminescence with good photostability and had good biocompatibility. The cell viability was about 95% in the presence of CS-CDs at a concentration of 400 μg mL^{-1}. Based on these findings, CS-CDs demonstrated their application in imaging cellular nuclei and tumors *in vivo*. In fact, other biomass materials that contain phenolic compounds could be treated in a similar way to convert under-evaluated biomass materials into high-value-added functional materials with excellent antioxidation and bioimaging performance. This work might open new opportunities to utilize phenolic-containing biomass materials correctly. Here, phenolic extracts of coffee bean shells were used to prepare carbon dots (CS-CDs) *via* a cheap, energy-saving, mild molecular aggregation method.

Conflicts of interest

There are no conflicts to declare.

Acknowledgements

Notes and references

1 Y.-J. Wang, H. Dong, G.-M. Lyu, H.-Y. Zhang, J. Ke, L.-Q. Kang, J.-L. Teng, L.-D. Sun, R. Si and J. Zhang, *Nanoscale*, 2015, **7**, 13981–13990.

2 S.-S. Chee and J.-H. Lee, *J. Mater. Chem. C*, 2014, **2**, 5372–5381.

3 L. Han, L.-B. Du, A. Kumar, H.-Y. Jia, X.-J. Liang, Q. Tian, G.-J. Nie and Y. Liu, *Biomaterials*, 2012, **33**, 8517–8528.

This journal is © The Royal Society of Chemistry and the Chinese Chemical Society 2018

4 S. Park, J. Yoon, S. Bae, M. Park, C. Kang, Q. Ke, D. Lee and P. M. Kang, *Biomaterials*, 2014, **35**, 5944–5953.

5 F. G. Calvo-Flores and J. A. Dobado, *ChemSusChem*, 2010, **3**, 1227–1235.

6 S. Wu and H. J. Butt, *Adv. Mater.*, 2016, **28**, 1208–1226.

7 G. Chen, J. Shen, T. Y. Ohulchanskyy, N. J. Patel, A. Kutikov, Z. Li, J. Song, R. K. Pandey, H. Ågren and P. N. Prasad, *ACS Nano*, 2012, **6**, 8280–8287.

8 Z. Chen, R. Thiramanas, M. Schwendy, C. Xie, S. H. Parekh, V. Mailänder and S. Wu, *Small*, 2017, **13**, 1613–6829.

9 D. Yang, Z. Hou, Z. Cheng, C. Li and J. Lin, *Chem. Soc. Rev.*, 2015, **44**, 1416–1448.

10 L. Feng, F. He, G. Yang, S. Gai, Y. Dai, C. Li and P. Yang, *J. Mater. Chem. B*, 2016, **4**, 8000–8008.

11 X. Xue, S. Jin, C. Zhang, K. Yang, S. Huo, F. Chen, G. Zou and X.-J. Liang, *ACS Nano*, 2015, **9**, 2729–2739.

12 A. Wang, L. Cui, S. Debnath, Q. Dong, X. Yan, X. Zhang, R. V. Ulijn and S. Bai, *ACS Appl. Mater. Interfaces*, 2017, **9**, 21390–21396.

13 J. Tian, Q. Liu, A. M. Asiri, K. A. Alamry and X. Sun, *ChemSusChem*, 2014, **7**, 2125–2130.

14 C.-B. Ma, Z.-T. Zhu, H.-X. Wang, X. Huang, X. Zhang, X. Qi, H.-L. Zhang, Y. Zhu, X. Deng and Y. Peng, *Nanoscale*, 2015, **7**, 10162–10169.

15 F. Niu, Y. Xu, M. Liu, J. Sun, P. Guo and J. Liu, *Nanoscale*, 2016, **8**, 5470–5477.

16 Z. Peng, E. H. Miyanji, Y. Zhou, J. Pardo, S. D. Hettiarachchi, S. Li, P. L. Blackwelder, I. Skromne and R. M. Leblanc, *Nanoscale*, 2017, **9**, 17533–17543.

17 W. Qin, D. Ding, J. Liu, W. Z. Yuan, Y. Hu, B. Liu and B. Z. Tang, *Adv. Funct. Mater.*, 2012, **22**, 771–779.

18 Z. Zhu, J. Qian, X. Zhao, W. Qin, R. Hu, H. Zhang, D. Li, Z. Xu, B. Z. Tang and S. He, *ACS Nano*, 2015, **10**, 588–597.

19 A. Sachdev and P. Gopinath, *Analyst*, 2015, **140**, 4260–4269.

20 S. Zhao, M. Lan, X. Zhu, H. Xue, T.-W. Ng, X. Meng, C.-S. Lee, P. Wang and W. Zhang, *ACS Appl. Mater. Interfaces*, 2015, **7**, 17054–17060.

21 W. Li, Z. Zhang, B. Kong, S. Feng, J. Wang, L. Wang, J. Yang, F. Zhang, P. Wu and D. Zhao, *Angew. Chem., Int. Ed.*, 2013, **52**, 8151–8155.

22 L. Cao, X. Wang, M. J. Meziani, F. Lu, H. Wang, P. G. Luo, Y. Lin, B. A. Harruff, L. M. Veca and D. Murray, *J. Am. Chem. Soc.*, 2007, **129**, 11318–11319.

23 S. Zhu, Q. Meng, L. Wang, J. Zhang, Y. Song, H. Jin, K. Zhang, H. Sun, H. Wang and B. Yang, *Angew. Chem.*, 2013, **125**, 4045–4049.

24 C. Ding, A. Zhu and Y. Tian, *Acc. Chem. Res.*, 2013, **47**, 20–30.

25 S. Y. Lim, W. Shen and Z. Gao, *Chem. Soc. Rev.*, 2015, **44**, 362–381.

26 K. Jiang, S. Sun, L. Zhang, Y. Lu, A. Wu, C. Cai and H. Lin, *Angew. Chem., Int. Ed.*, 2015, **54**, 5360–5363.

27 T. Feng, X. Ai, G. An, P. Yang and Y. Zhao, *ACS Nano*, 2016, **10**, 4410–4420.

28 Z. Yang, M. Xu, Y. Liu, F. He, F. Gao, Y. Su, H. Wei and Y. Zhang, *Nanoscale*, 2014, **6**, 1890–1895.

29 F. Zhou, T.-H. Leng, Y.-J. Liu, C.-Y. Wang, P. Shi and W.-H. Zhu, *Dyes Pigm.*, 2017, **142**, 429–436.

30 X. Zhang, M. Jiang, N. Niu, Z. Chen, S. Li, S. Liu and J. Li, *ChemSusChem*, 2018, **11**, 11–24.

31 N. Niu, Z. Ma, F. He, S. Li, J. Li, S.-X. Liu and P. Yang, *Langmuir*, 2017, **33**, 5786–5795.

32 M. P. Kahkonen, A. I. Hopia, H. J. Vuorela, J.-P. Rauha, K. Pihlaja, T. S. Kujala and M. Heinonen, *J. Agric. Food Chem.*, 1999, **47**, 3954–3962.

33 N. Balasundram, K. Sundram and S. Samman, *Food Chem.*, 2006, **99**, 191–203.

34 P. S. Murthy and M. M. Naidu, *Food Bioprocess Technol.*, 2012, **5**, 897–903.

35 A. Moure, J. M. Cruz, D. Franco, J. M. Domínguez, J. Sineiro, H. Domínguez, M. a. J. Núñez and J. C. Parajó, *Food Chem.*, 2001, **72**, 145–171.

36 Z. Liang, L. Zeng, X. Cao, Q. Wang, X. Wang and R. Sun, *J. Mater. Chem. C*, 2014, **2**, 9760–9766.

37 X. Wang, Y. Guo, D. Li, H. Chen and R.-c. Sun, *Chem. Commun.*, 2012, **48**, 5569–5571.

38 X. Zhao, M. Li, H. Dong, Y. Liu, H. Hu, Y. Cai, Y. Liang, Y. Xiao and M. Zheng, *ChemSusChem*, 2017, **10**, 2626–2634.

39 Y. Shi, Y. Na, T. Su, L. Li, J. Yu, R. Fan and Y. Yang, *ChemSusChem*, 2016, **9**, 1498–1503.

40 A. Suryawanshi, M. Biswal, D. Mhamane, R. Gokhale, S. Patil, D. Guin and S. Ogale, *Nanoscale*, 2014, **6**, 11664–11670.

41 Y. Deng, X. Feng, M. Zhou, Y. Qian, H. Yu and X. Qiu, *Biomacromolecules*, 2011, **12**, 1116–1125.

42 F. Würthner, T. E. Kaiser and C. R. Saha-Möller, *Angew. Chem., Int. Ed.*, 2011, **50**, 3376–3410.

43 H. Zhang, X. Zheng, N. Xie, Z. He, J. Liu, N. L. Leung, Y. Niu, X. Huang, K. S. Wong and R. T. Kwok, *J. Am. Chem. Soc.*, 2017, **139**, 16264–16272.

44 P. Sharma, M. Majdi Yazdi, A. Merriman, R. A. Manderville and S. D. Wetmore, *Chem. Res. Toxicol.*, 2015, **28**, 782–796.